Multiphase lattice metamaterials with enhanced mechanical performance

Fatih Usta[1,*], Fabrizio Scarpa[2], Halit S. Türkmen[1], Peter Johnson[3], Adam W. Perriman[4], Yanyu Chen[5]

[1] Faculty of Aeronautics and Astronautics, Istanbul Technical University, Istanbul, Turkey

[2] Bristol Composites Institute (ACCIS), University of Bristol, Bristol, United Kingdom

[3]Department of Chemistry, University of Oxford, Oxford, United Kingdom

[4]School of Cellular and Molecular Medicine, Faculty of Biomedical Sciences, University of Bristol, Bristol, United Kingdom

[5]Department of Mechanical Engineering, University of Louisville, Louisville, USA

[*]Corresponding author, E-mail address: ustaf@itu.edu.tr (F. Usta)

Abstract

We describe here the quasi-static crushing behavior of novel classes of multiphase (hybrid) hierarchical lattice metamaterials. The first class is represented by a hybrid architecture combining a hierarchical honeycomb with polyurethane foam filler, while the second is a multiphase structure produced by injecting an alginate hydrogel into the hierarchical voids of the honeycomb metamaterial. Twelve different auxetic (i.e., negative Poisson's ratio) and non-auxetic metamaterial architectures have been 3D printed and subjected to edgewise compression crushing loading. A parametric numerical analysis has been also performed using validated Finite Element models to identify best metamaterial architecture configurations. Configurations filled with the hydrogel showed a significant stabilization of the deformation mechanism during large deformation edgewise compression. The use of metamaterials designs with internal slots and round in the ribs also filled by polyurethane rigid (PUR) semi-reticulated foam feature however significant increases in terms of specific stiffness, mean crushing force, strength and energy absorption. The enhancement is particularly evident for the hybrid lattice metamaterials auxetic configurations.

Keywords: Mechanical metamaterials, hierarchical honeycombs, auxetics, multiphase, hybrid, quasi-static crushing behavior.

1. Introduction

Mechanical metamaterials and auxetics have a wide range use in engineering applications due to their lightweight characteristics, large energy absorption, heat insulation, tailorable stiffness and strength. Auxetic materials exhibit negative Poisson's ratio (NPR) under tensile or compressive loading and are represented across a wide range of materials, which include cellular solids, microporous polymers, composites and molecular assemblies. Typical unit cell configurations of auxetic materials are the re-entrant [1-7], arrowhead [7-11], chiral [6], rhombic [9-12], star-shaped [13] and tetra-petals [14] configurations. Here we focus on re-entrant (butterfly) structures, which are one of the most common and earliest auxetic materials proposed. The butterfly shape morphology is based on arranging the inclined rib if the hexagonal honeycomb at a negative angle [15]. Several pioneering studies related to auxetic cellular structures have shown advantages superiority over classical cellular configurations in terms of mechanical properties, which results from the interplay between the geometry of the unit cells of those lattices and the characteristics of their core materials [15-24].

Re-entrant auxetic cellular structures have been investigated under different loading conditions (indentation, flatwise and edgewise compressive loading). A considerable amount of work has been carried out to understand the in-plane compressive behavior of re-entrant honeycombs. Dong *et al.* [25] evaluated the effects of the wall thickness and negative Poisson's ratio (NPR) on the mode shapes and crushing stress of re-entrant honeycombs. Thick walled honeycombs tended to contract towards the center of lattice, unlike thin walled honeycombs that showed local contractions on the edges. The NPR had insignificant effects on the plateau stresses. Xiao *et al.* [26] demonstrated that the NPR and deformation modes significantly affected the behavior of the lattices at different compression speeds. Tatlier [27] examined the effects of the loading orientation in re-entrant honeycombs to quantify the absorbed energy. The re-entrant honeycomb with 90^0 alignment exhibited better energy absorption capacity compared to the other loading directions. Liu *et al.* [28] indicated that irregular re-entrant honeycombs dissipated more energy and exhibited higher compressive strength before densification than conventional hexagonal honeycombs.

Recent works have shown that specific architectures of unit cells can enhance the mechanical properties and energy absorption capacity of cellular structures. Tan *et al.* [29] investigated two re-entrant hierarchical honeycombs including unit cells with regular hexagon and equilateral triangle substructures. Chen *et al.* [30] showed that hierarchical cellular configurations created by replacing cell walls with triangular lattices provided progressive failure modes, higher energy absorption and stiffness under uniaxial loading. Ingrole *et al.* [1] developed a new hybrid-auxetic-strut structure combining re-entrant auxetic and regular honeycomb unit cells. The configuration showed an improved energy absorption capacity and strength under compression loading and reduced stress concentration under large deformations because of the custom struts designs. Alomarah *et al.* [31] investigated the compressive properties of re-entrant chiral auxetic structures (RCA) combining topological features of re-entrant and chiral honeycombs. The RCA structure could provide more specific energy absorption and strength than other types of honeycombs depending upon the loading direction.

All types of materials can display auxetic behavior if they take the shape of any auxetic cellular form and mechanical properties can be improved by arranging dimensions or shapes. In addition to this, auxetic structures with the combination of two or more materials can provide another solution to enhance the overall mechanical properties. Studies on auxetics composite materials have significantly increased over the past decade [32]. Ge *et al.* [33] numerically investigated the compression behavior of 3D auxetic textile structures composing of weft, yarn and stitch yarns reinforcements. Jayanty *et al.* [34] reported auxetic behavior of some polymer nanocomposites with carbon nanofibers. Jopek and Strek [35] investigated the thermomechanical behavior (geometry of fiber and thermal effects on materials) of auxetic composites built from two constitutive materials. Previously, composites made of auxetic lattices as reinforcement and surrounding viscoelastic matrix have been developed by Scarpa *et al.* [36] and Gandhi's Group [37, 38]. Viscoelastic inserts bridging segments of the honeycomb cell walls have been also used to increase damping and energy dissipation [39, 40]. Sloan et al. [41] discussed the effects of the starting angle of a wrap fiber, diameter ratio of wrap to core fibers and the inherent Poisson's ratio of the fibers on their novel auxetic textile composites. Quan [42] showed that continuous fiber reinforced thermoplastic composite auxetic honeycomb had extremely high compressive stiffness and energy absorption capacity than the pure polylactic acid (PLA) re-entrant honeycomb. Subramani *et al.* [43] investigated the mechanical behavior of five different auxetics by changing the structural cell angle and using core reinforced braided composite rods. Xu *et al.* [44] have shown that non-Newtonian fluid could improve low-velocity impact and compression resistance of composite structures. Shear thickening fluids provide for example a synergistic effect with auxetic warp-knitted

spacer fabrics and could increase energy absorption of the composites due to the shear thickening transition. Large energy absorption under impact has been also recently observed when shear thickening (Non-Newtonian) fluids have been used as through-the-thickness fillers in hexagonal honeycomb sandwich panels [45].

Differently from existing auxetic lattice and composite designs, this study introduces a novel type of composite open cells honeycombs with the PLA plastic reinforcements, hydrogel and polyurethane rigid (PUR) foam over a hierarchical cellular platform presented in [46] consisting of one phase material system only. The compression behavior of novel class of hierarchical (slotted) and asymmetrical edge cellular shape honeycombs with auxetic and non-auxetic configurations was originally described in [46]. The presence of the slotted and asymmetric cells contributed to increase strength, stiffness and energy absorption capacity of the samples compared to conventional types of cellular structures. To the best of the Authors' knowledge, the present study presents for the first time hydrogels and other multiphase material systems used as core constituents within auxetic and hierarchical lattice configurations.

In this work we describe the design, manufacturing, characterization and mechanical compression of these novel multifunctional auxetic structures. Effective compressive stiffness, strength and specific energy absorption capabilities of the structures are here discussed. The advantages and disadvantages of our novel designs are also evaluated. The experimental results of the hybrid and multiphase types of the new composite hierarchical structures are compared with the analogous results from samples with their internal configuration made of full solid materials. The results show that the novel hybrid and hierarchical structures provide higher relative strength, stiffness and specific energy absorption than the other configurations. In addition, the novel multiphase structures tend to reduce instabilities occurring during the deformation of auxetic cellular structures when loaded along a particular direction. Finally, a parametric Finite Element (FE) analysis study has been also carried out to improve the crashworthiness performance of the novel hybrid structure by changing number of slots and defining round on the corners of the slots and foams. The results of the FE analysis show that the combination of rounded corners and increase of the number of slots in the hierarchical cellular structure gives rise to a significant increase in the mechanical performance of the hybrid and multifunctional lattice.

2. Design methodology and manufacturing processes

2.1. Unit cell designs

The baseline cell architectures considered in this work are re-entrant configurations with asymmetrical units along the edges and the perforated rib lattice configuration based on controlled porosity of the 3D printing process [46]. We consider here two types of multiphase material architectures for the ribs of those lattice configurations. The first combines a solid slotted (deterministic porosity) made of PLA and filled with a non-Newtonian gel (hydrogel). The type of hydrogel used here is alginate gel. The second is related to a type of hybrid structure made of PUR foam added into slots (deterministic pores) of the PLA-made samples.

In terms of unit cell geometry, our designs are classified as hexagonal, re-entrant and asymmetric re-entrant. The design parameters of the unit cell are as the height H, the thickness t of the struts, the length l of the inclined strut, the internal cell angle θ and the out of plane thickness b of the struts (Figure 1). The dimensions of those parameters used for the 3D printed samples are h=30 mm, t=3 mm, l=15 mm, θ=60° and b=20 mm. Dimensions and number of cells in each specimen are the same, except for the case of the asymmetric unit cells in which the length of the rib is l=16.96 mm and the inclined angle of the edge side facing outwards is 50°.

The hierarchical (slotted) structures are designed by leaving two small gaps along the thickness of the ribs. The thickness of the struts in the slotted cells is 0.8 mm.

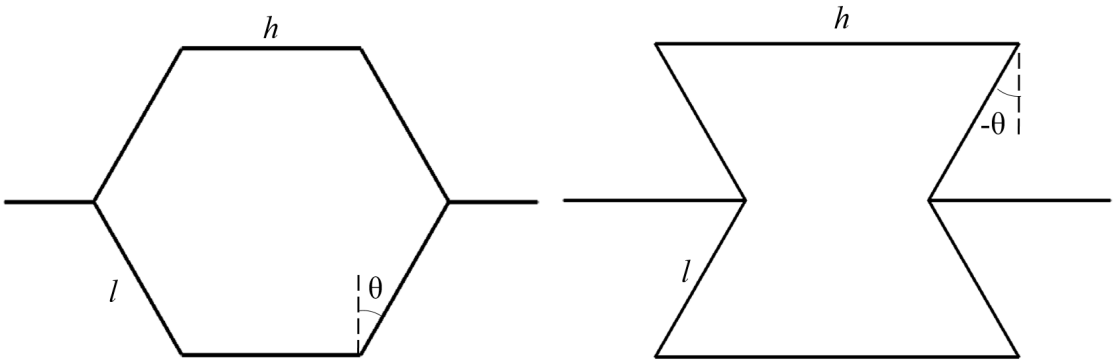

Figure 1: Conventional and re-entrant honeycomb structures.

Figure 2 shows unit cells with bulk (fully filled ribs) thickness, slotted and composite cellular structures are listed considering hexagonal, and symmetric/asymmetric re-entrant types.

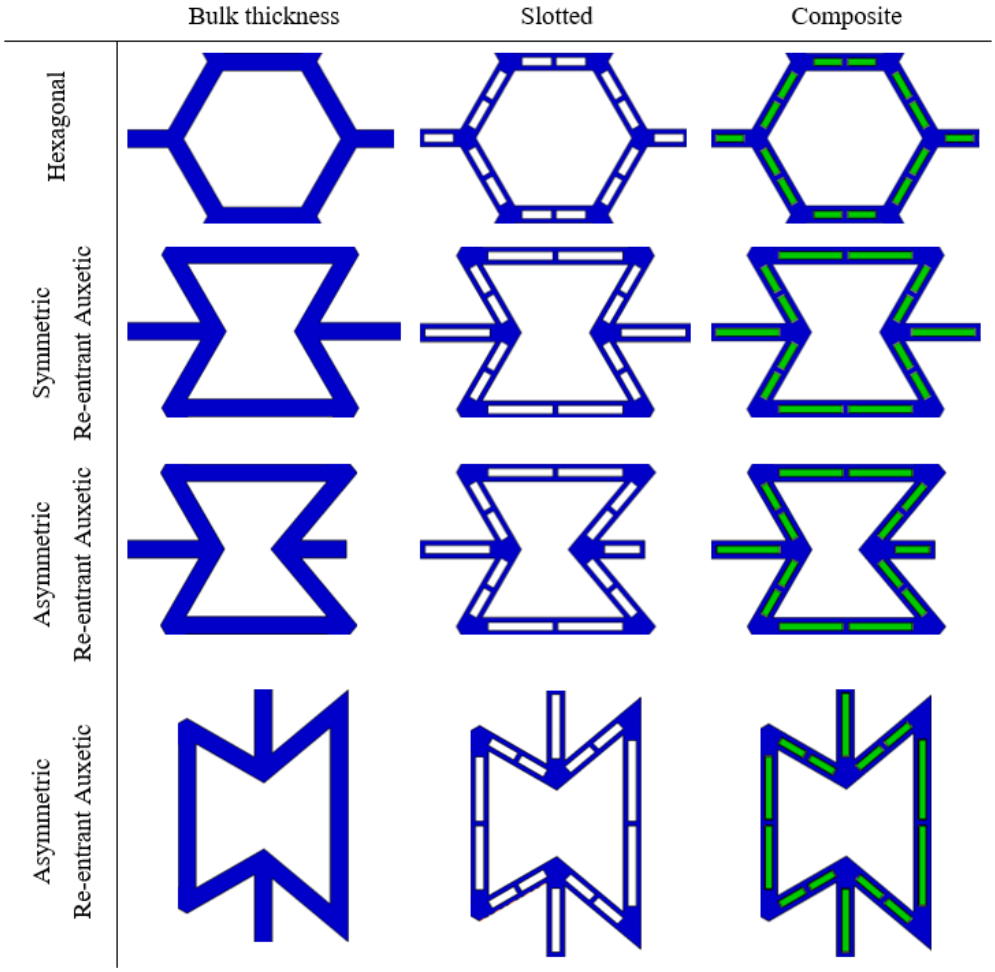

Figure 2: Bulk thickness, hierarchical (slotted) and composite (PUR foam and hydrogel) cells.

2.2. 3D printing of the PLA plastic slotted samples

The PLA-made slotted samples have been printed using a Raise3D N1 3D machine based on fused deposition modeling. The CAD stl design was imported into the Ideamaker 3D printer slicing software. This software converted the stl into a gcode file by selecting two outer shells, 100% filling ratio and ±45° infill angles. Specimens consisting of 5 x 4 (width x height) number of unit cells have been printed at 225 °C of extruder temperature, with 65 °C of heated bed temperature and 0.2 mm layer height.

2.3. PLA-made hierarchical cellular honeycombs filled with hydrogel

A multi-component hydrogel was used as a core constituent within the auxetic and hierarchical lattice configurations to stabilize the whole deformation of the lattices during large geometric and material nonlinear loading, and also to verify potential increase in terms of energy absorption.

Characterization and preparation of the hydrogel used has been previously described [47]. Briefly, the hydrogel formulation consists of sodium alginate (alginate) and a non-ionic surfactant, Pluronic F127 (F127). A 10% w/v alginate solution was prepared through centrifugation of sodium alginate powder (Sigma Aldrich, UK) with Dulbecco's Modified Eagle's Medium (DMEM, Sigma Aldrich, UK), using a dual asymmetric centrifuge (DAC 150.1 FV, SpeedMixer, UK) at 3500 RPM for 5 minutes. A 40 % w/v solution of F127 in Phosphate Buffered Saline (PBS, Sigma Aldrich, UK) was autoclaved at 121 °C for 40 minutes, then cooled to 4 °C and stored for up to a week before use. The working gel formulation was 6 wt% w/v alginate, 13 wt% w/v F127, and was achieved by mixing alginate and F127 solutions with a DAC at 3500RPM for 30 seconds. Gels were transferred to 20ml syringes (Terumo Corporation, Japan) after mixing and injected into slots within PLA structures (Figure 3a). Then, gel-containing PLA structures were immersed in a 100mM $CaCl_2$ bath for 10 minutes (Figure 3b), prepared by dissolving calcium chloride powder (Sigma Aldrich, UK) in deionized water. The $CaCl_2$ bath crosslinked the alginate gel component, whilst allowing the F127 component to dissolve and diffuse out of the gel structure. The resulting gel structure is a macroporous alginate hydrogel.

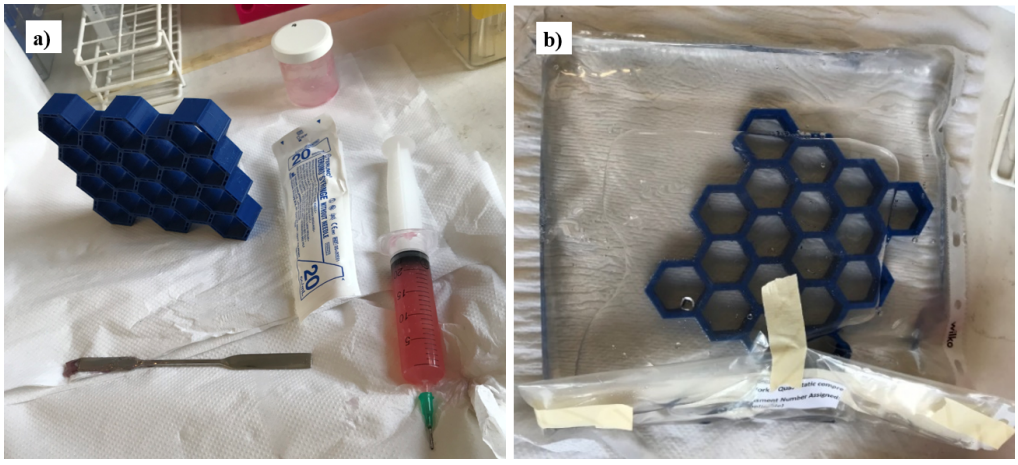

Figure 3: a) Hydrogel injection into the slots, b) $CaCl_2$ bath of hexagonal slotted lattice.

2.4. PLA-made hierarchical cellular honeycombs filled with PUR foam

PUR foam blocks (density 69 kg m^{-3}) were cut by using a CNC machine in accordance with the dimensions of gaps in the architectural structures. The foam cuts were then manually positioned into the gaps one by one. Each PLA-made sample contains 150 gaps and the size of

these gaps can differentiate according to the position of ribs in the unit cell and configuration types. An example of a filled slotted re-entrant lattice is shown in Figure 4.

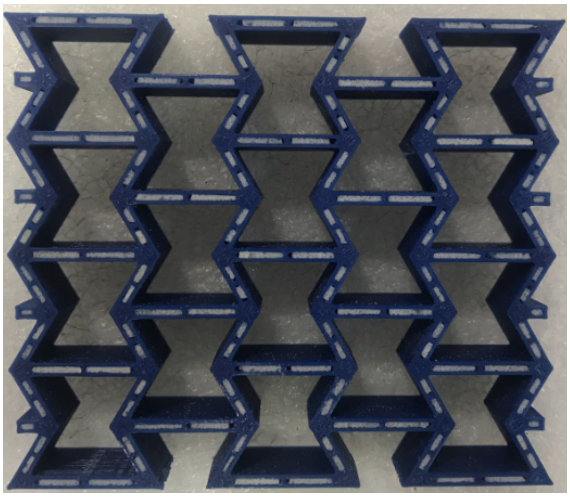

Figure 4: Slotted re-entrant honeycomb filled with PUR foam.

3. Material properties of PLA plastics and PUR foam

3.1. Tensile tests of PLA plastics

Six dogbone specimens have been printed following the ASTM D638-14 test standard [48] by using a Raise3D N1 machine. Tensile tests have been performed using an Instron 25 kN test machine. Stress-strain curves of the samples have been obtained, and the Poisson's ratio was measured from the in-plane displacements of target points recorded with a video gauge system. The average Young's modulus of the PLA samples is 4.6 ±0.1 GPa, the ultimate strength is 49±1 MPa, the yield strength is 45±2 MPa, the density is 1.45 gr/cm^3 and the Poisson's ratio is 0.36 ±0.02. The engineering stress–strain curves of the specimens are plotted in Figure 5.

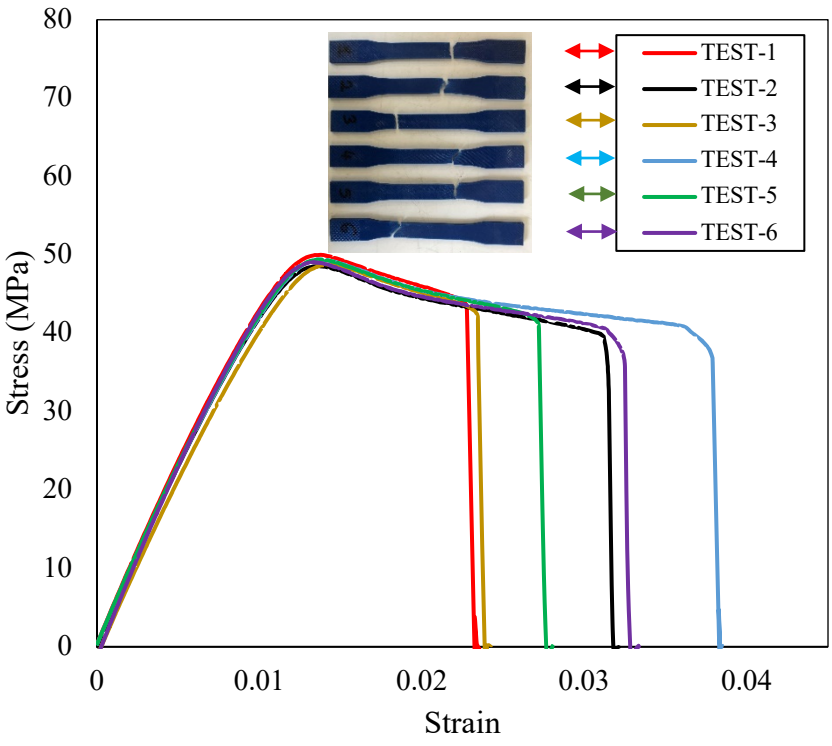

Figure 5: Stress-strain curves of the PLA plastic [46].

3.2. Compression tests of PUR foam

Compression tests on the PUR semi-reticulated cell foam with the components organic resins of polyol and isocyanate (ESPOL Sponge and Chemical Industry Ltd. Co., Turkey) have been performed on cubic samples (5x5x5 cm) prepared in accordance to the ASTM D1621-91 standard [49] by using an MTS Universal test machine (Figure 6). Compression tests in displacement control mode were carried out parallel to the three axis-directions with crosshead speeds of 2.5, 25 and 100 mm/min corresponding to the strain rates of $8.33x10^{-4}$, $8.33x10^{-3}$ and $3.33x10^{-2}$ s^{-1} in order to investigate the anisotropy of the foam material and its strain rate dependency [50]. Each case was repeated by testing 5 identical test specimens at different strain rates and different loading directions. 45 cubic foam were tested in order to determine mechanical properties of PUR foam.

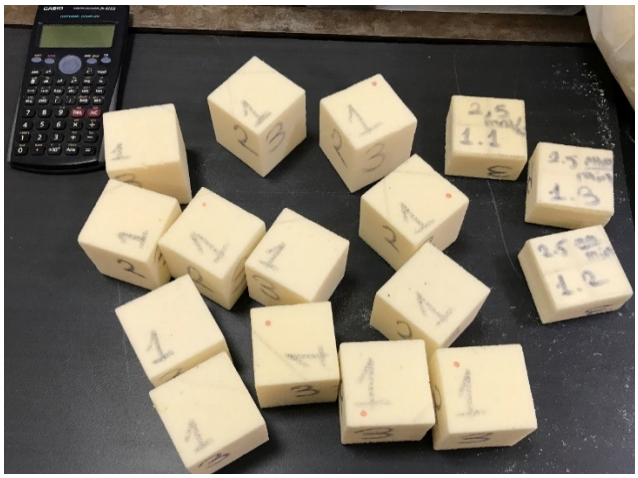

Figure 6: Cubic PUR foam test samples.

Loading directions were coded as 1, 2 and 3 on the surfaces of samples which represented material directions of cubic test samples (Figure 7).

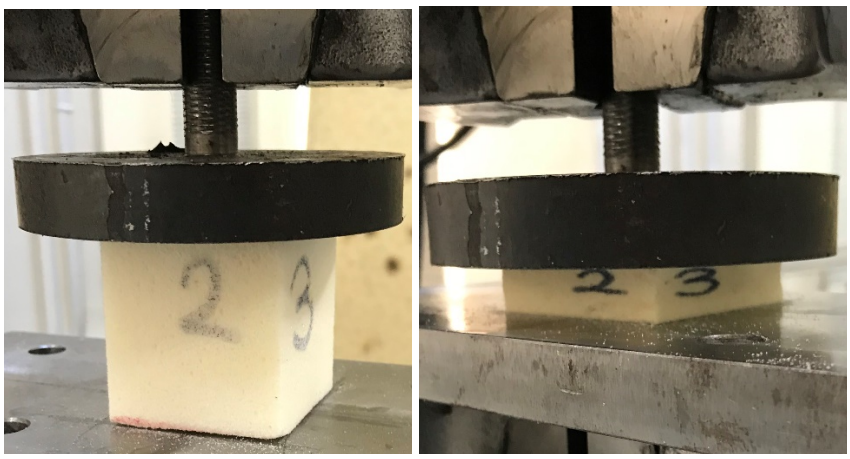

Figure 7: Compression test of the PUR foam.

The average stress-strain curves of the specimens are plotted according to different strain rates and loading directions in Figure 8. The results show that each curve contains typically three distinct regions (as expected): a linear elastic and a plateau followed by densification.

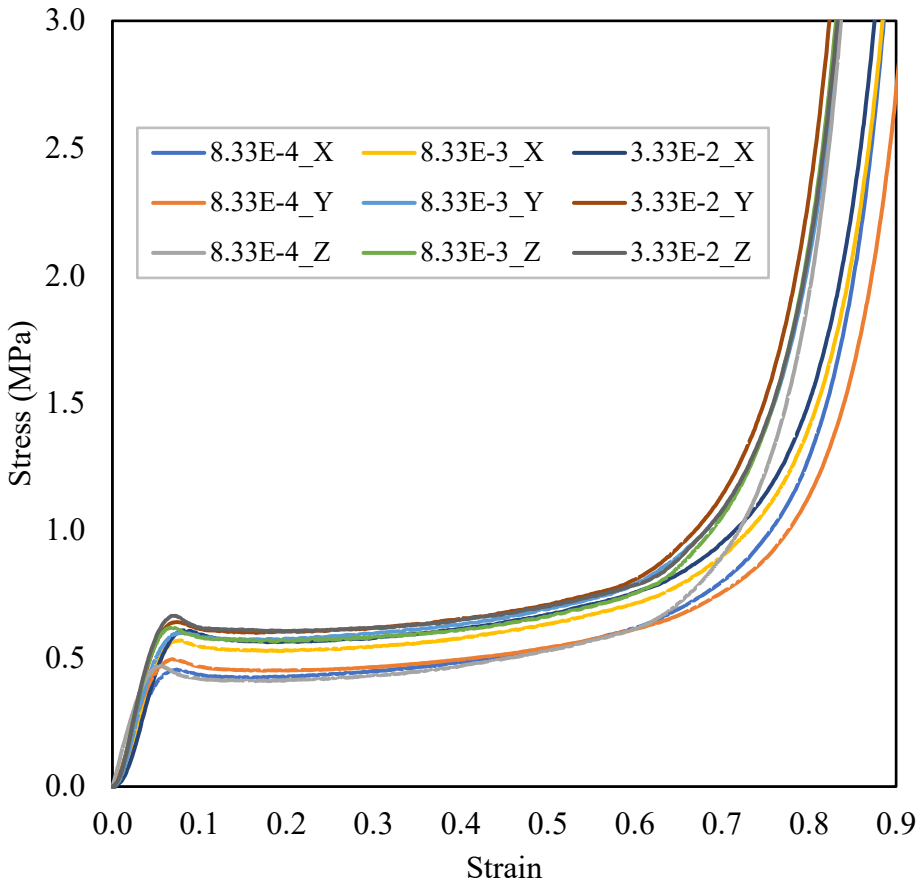

Figure 8: Comparison average stress-strain curves of the foams at different strain rates.

The linear elastic properties of each test were determined according to stress vs strain curves in Figure 8 and Young's modulus, plateaus onset stress and corresponding strains are shown in Table 1.

Table 1: Material properties of PUR foams.

	ε	E (MPa)	ε	σ_{pl} (MPa)
2.5-X	0.069	10.294	0.073	0.459
2.5-Y	0.005	10.278	0.073	0.499
2.5-Z	0.005	11.381	0.067	0.474
25-X	0.004	10.338	0.084	0.574
25-Y	0.006	10.966	0.084	0.604
25-Z	0.006	11.294	0.083	0.626
100-X	0.006	11.060	0.085	0.613
100-Y	0.026	11.807	0.083	0.647
100-Z	0.019	11.509	0.085	0.670

Table 1 clearly indicates that there is no remarkable difference between the values of the Young's moduli, no matter which loading direction or strain rate is considered. The stress corresponding to the plateau onset is however strain rate dependent, with a maximum discrepancy of ~ 41% between the analogous values along the z-direction when passing from

25 mm min-1 to 100 mm min-[1]. For the continuation of our study we have adopted the results of the samples tested at 2.5 mm/min.

4. Experimental compression tests

The compression tests were carried out using an INSTRON Roell Amsler Test Machine with a 25 kN load cell at the speed of 3 mm/min. The specimens were compressed along the *x* and *y*-material directions in separate tests. The representative normalized stress vs strain curves of AEC re-entrant samples are indicated in Figure 9.

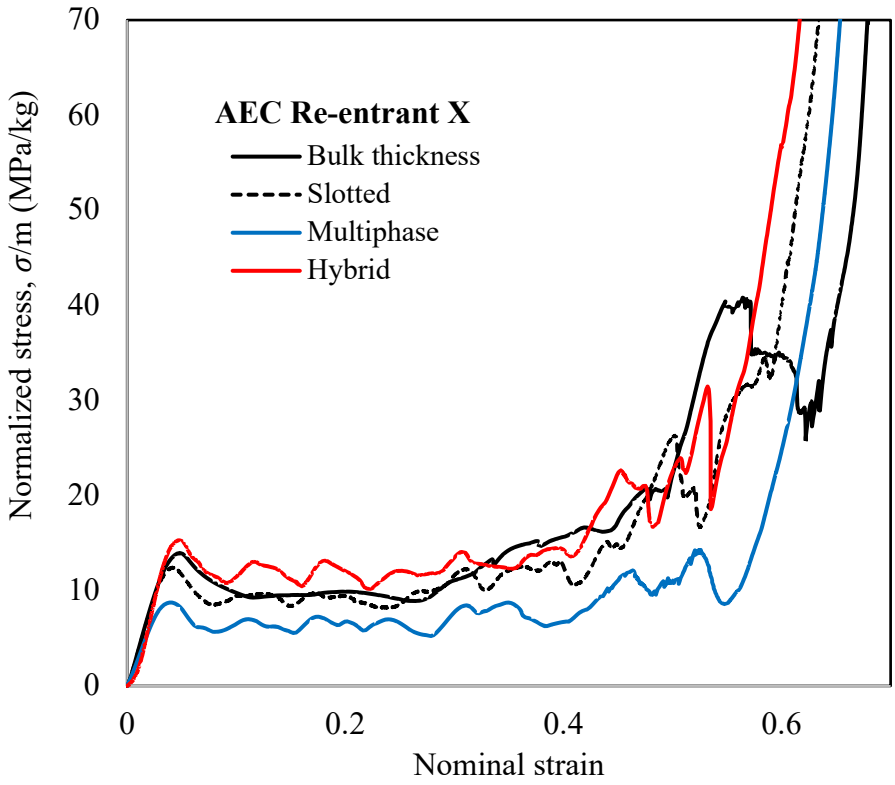

Figure 9: Stress vs. strain curves of re-entrant samples under compression along the x-direction: Bulk thickness (black), Slotted (dashed), Multiphase (blue) and Hybrid (red).

During the tests no out-of-plane displacements were observed. An Imetrum Video Gauge™ system was used to capture images of the in-plane deformations. Figures 10-15 show the deformation patterns related to the bulk thickness [46], slotted [46], multiphase and hybrid samples. The specimens are related to lattice configurations (hexagonal, re-entrant and AEC re-entrant), both loaded along the *x* and *y*-directions. Usta *et al.* [46] have previously shown how the deformation mechanism of the bulk thickness and slotted structures are dominated by the inclined ribs in the case of samples crushed along the *x*-direction. In a similar manner the deformation mechanism of the multiphase and hybrid samples appears to be dominated by the inclined ribs when loading along the same direction. Microbeams belonging to the first yielding cells of the multiphase and hybrid samples fail where the strain reaches a critical limit and densification starts at the strains of 0.708, 0.701, 0.508, 0.521, 0.601 and 0.580 for the hexagonal, re-entrant and AEC re-entrant multiphase and hybrid samples, respectively. The results indicate that all the hexagonal types possess similar collapse mechanisms, except for the bulk thickness samples that do not feature microcracks on the ribs.

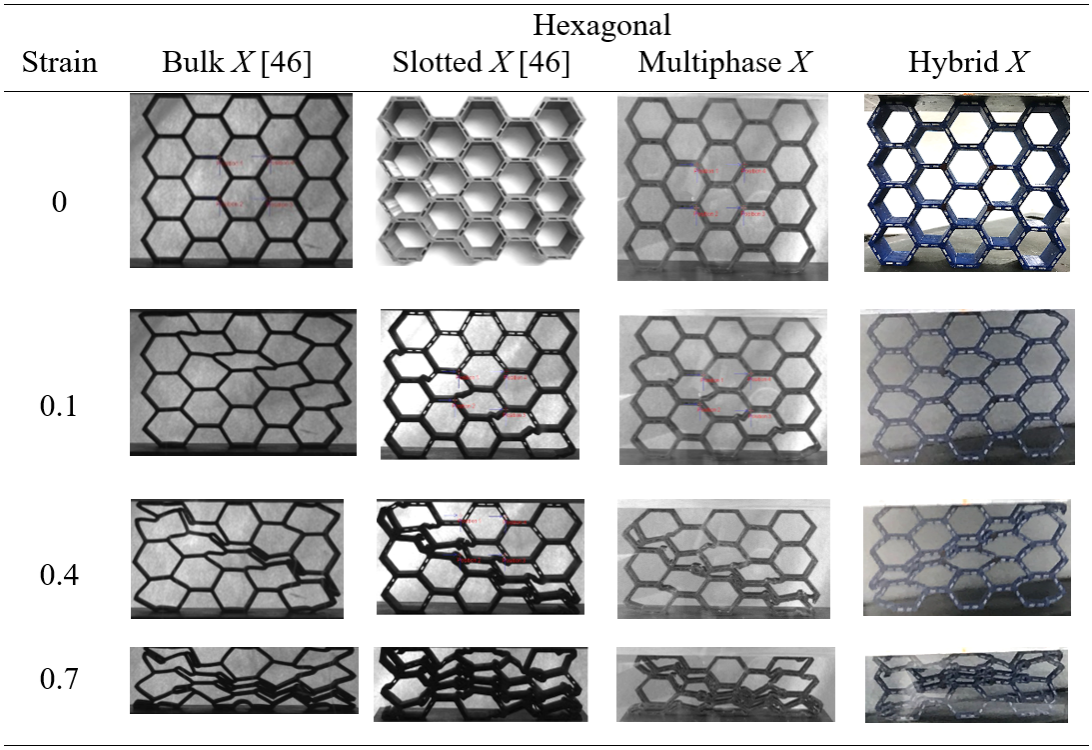

Figure 10: Deformation mechanisms of hexagonal honeycombs along the *x*-direction.

As expected, the auxetic structures (re-entrant and AEC re-entrant) show negative Poisson's ratio behaviors during the elastic deformation under compression loading along the *x*-direction. When stresses reach the onset of plateau stress, the deformation assumes a global buckling behavior due to the rotation of cells around the failed ribs. Usta *et al.* [46] have shown that slotted lattices possess advantages over bulk thickness configurations because of the reduction of global rotations during the deformation. This has also been observed in hierarchical lattice configurations evaluated by Chen *et al.* [30] and Yin *et al.* [51]. It is evident from observing Figure 11 that multiphase structures reduce significantly the global rotation of the samples during collapse and assume a more stable and progressive deformation because of the presence of the hydrogel. This is also valid and even more evident for the AEC re-entrant configurations shown in Figure 12, with the multiphase lattice type showing a clear progressive and almost parallel front of collapse without global rotations of the samples.

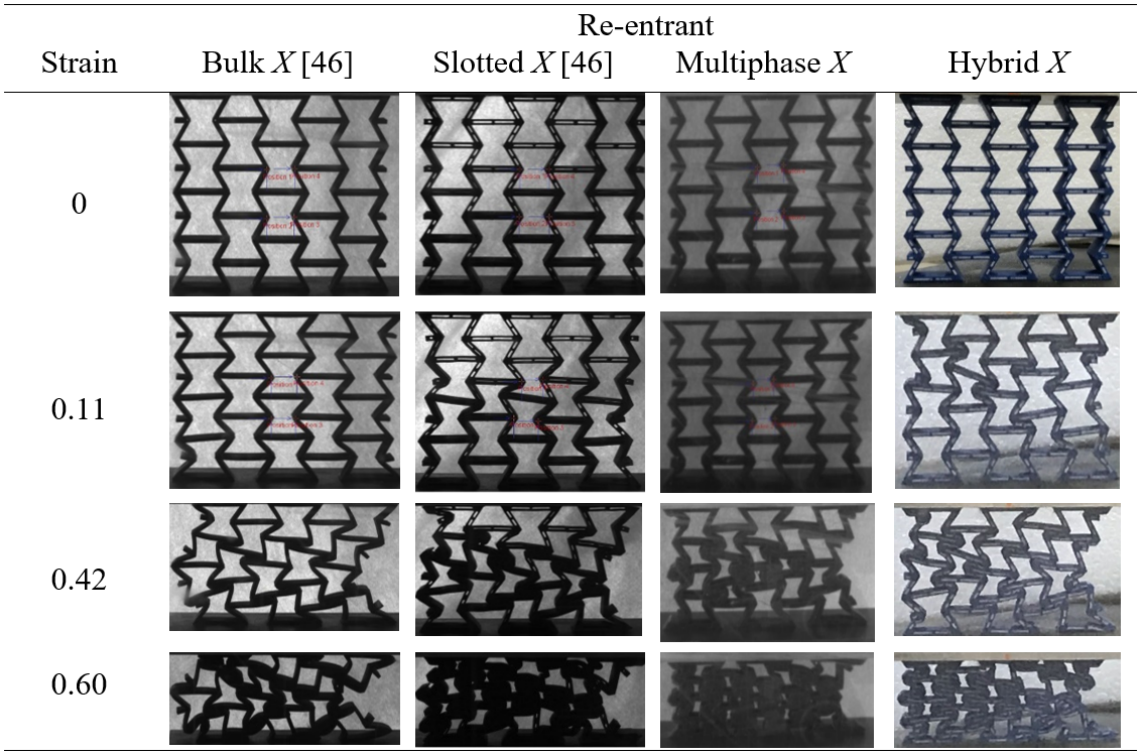

Figure 11: Deformation patterns of the re-entrant honeycombs along the *x*-direction.

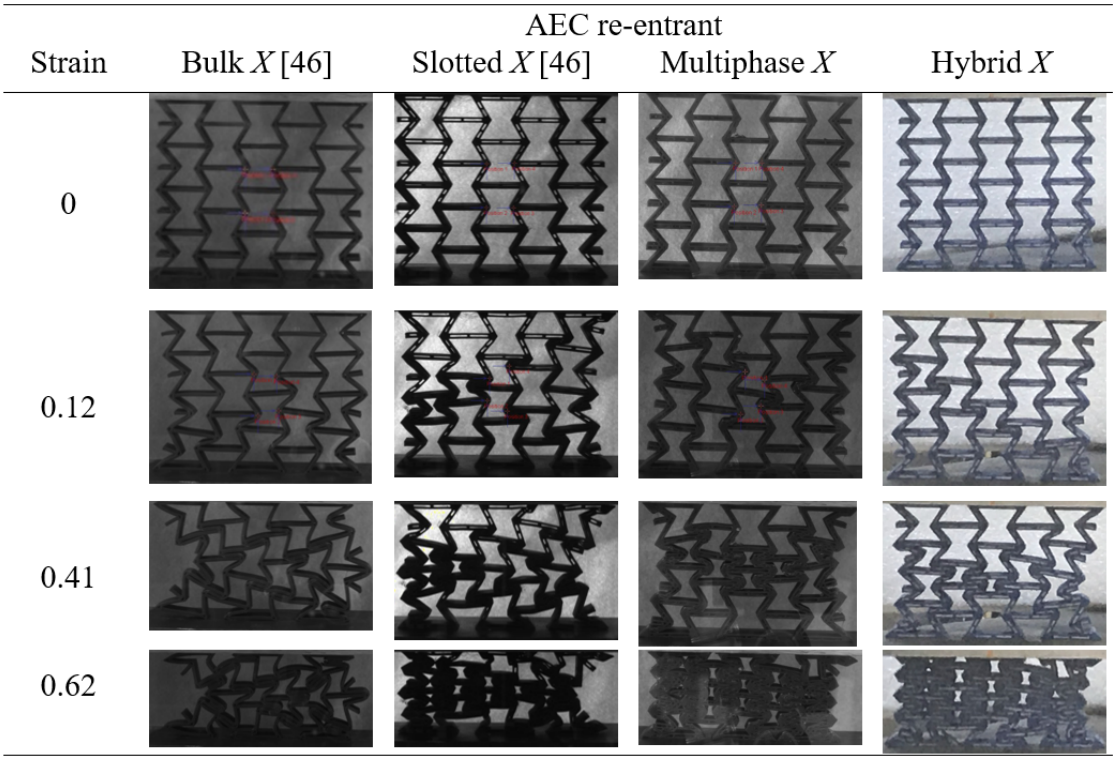

Figure 12: Deformation mechanisms of the AEC re-entrant honeycombs along the *x*-direction.

In the case of loading along the *y*-direction, the deformations of the vertical and inclined ribs both contribute to the global deformation of the honeycombs. Usta *et al.* [46] have shown that elastic buckling, plastic collapse and brittle failure are all mechanisms present during the deformation of the bulk thickness and slotted hexagonal samples. Multiphase and hybrid

samples exhibit similar deformation modes (Figure 13). Multiphase specimens seem here to feature a collapse front on cells close to the lower platen, while all the other samples tend to show the onset of the presence of this front towards the top of the specimen. This is an overall indication that the multiphase hexagonal samples appear to provide a more uniform transfer load during quasi-static crushing compared to the other configurations (bulk thickness included). In the re-entrant samples (Figure 14), the cells in the second and fourth rows of the slotted, multi-phase and hybrid samples tend to deform by beam buckling and brittle failure, while the bulk thickness samples tend to collapse by providing first a global rotation of the sample. Multiphase samples also fail by progressive front of buckling failure of the vertical ribs, but the overall compressive deformation towards densification is more uniform than the other configurations.

The collapse mechanism of the AEC re-entrant samples is different from the ones of the re-entrant samples when loading *y*-direction because of the presence of the edge asymmetric cells (Figure 15). The vertical ribs of asymmetric cells along the left and right sides are longer than those belonging to the internal cells. This AEC topology avoids the onset of an earlier plastic deformation of the second and fourth rows of the lattices, compared to the other configurations.

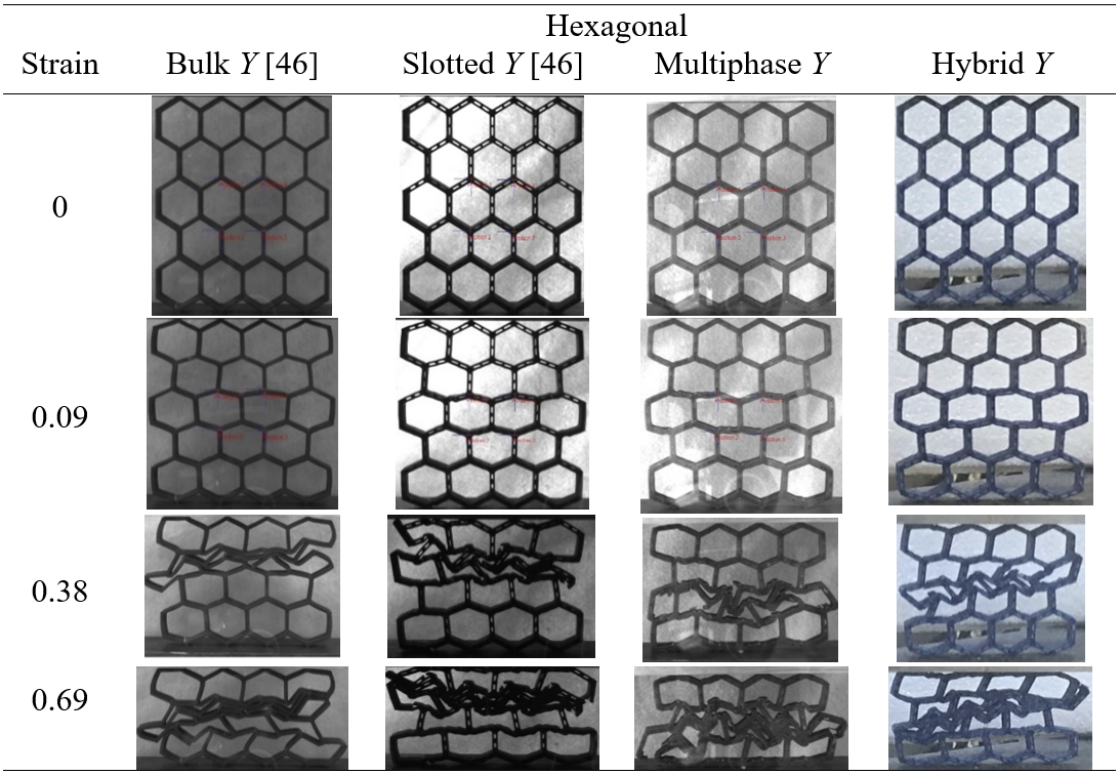

Figure 13: Deformation mechanisms of hexagonal honeycombs along the *y*-direction.

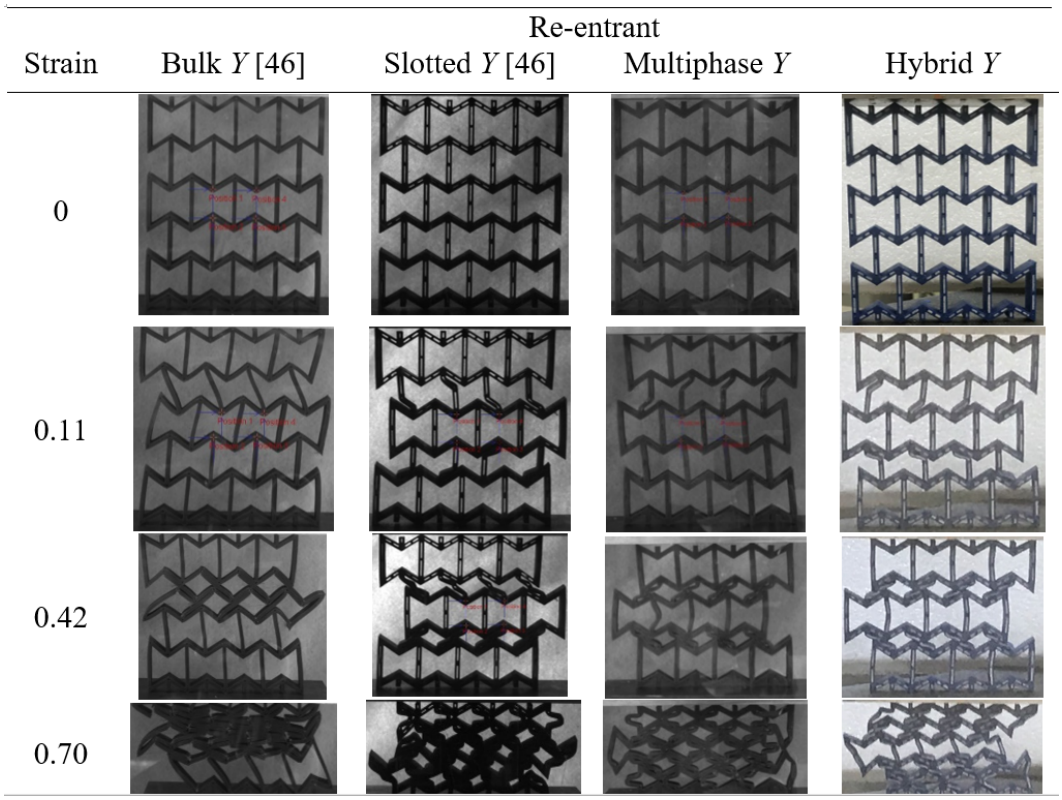

Figure 14: Deformation mechanisms of re-entrant honeycombs along the *y*-direction.

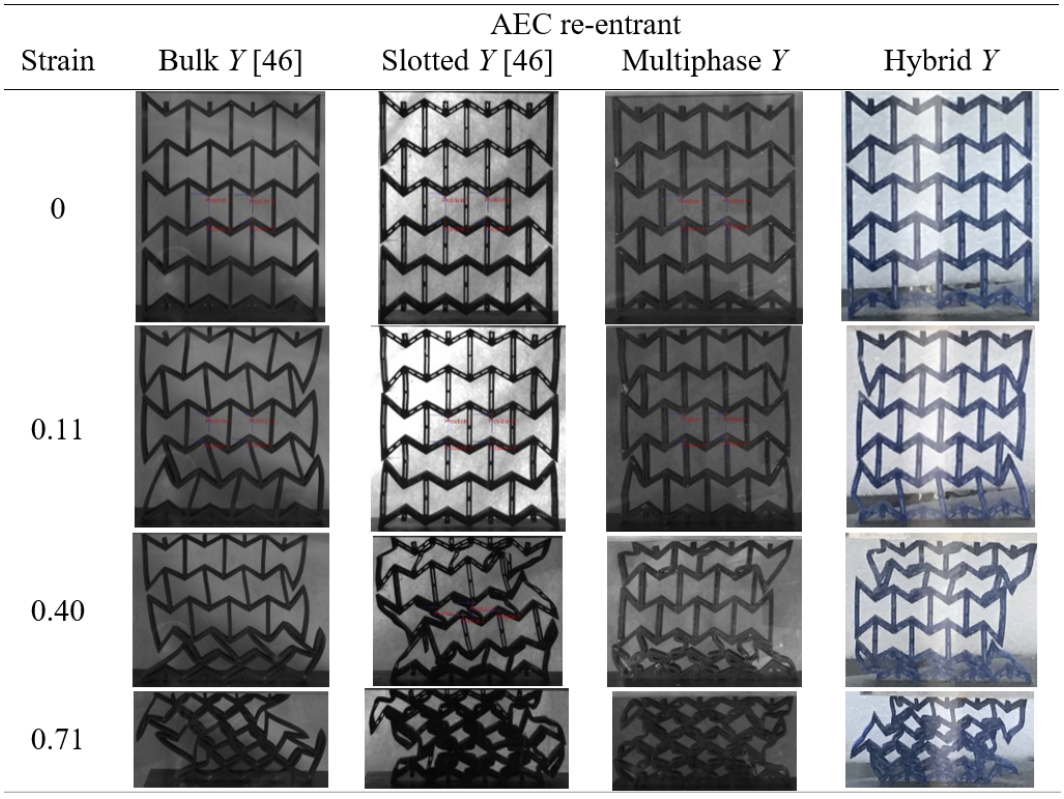

Figure 15: Deformation mechanisms of AEC re-entrant honeycombs along the *y*-direction.

5. Results and discussion

5.1. Metrics for benchmark

The results of compression tests were compared in terms of specific compressive modulus, strength, specific energy absorption and mean crushing force metrics defined as:

Specific compressive strength: $$\frac{Compressive\ stress}{Mass} = \frac{\sigma}{m} \quad (1)$$

Mean crushing force (MCF) $$\frac{Absorbed\ Energy}{Displacement} \quad (2)$$

Specific energy absorption (SEA): $$\frac{Absorbed\ energy}{Mass} \quad (3)$$

Specific compressive modulus $$\frac{Compressive\ modulus}{Mass} = \frac{E}{m} \quad (4)$$

Although in [46] the specific compressive strength has been calculated as the ratio between the compressive strength at densification point and the relative density, this formulation has been revised here by considering the total mass, so to cater for multiple types of materials in hybrid and multiphase samples. The formulation of the relative density used in [46] for comparison was expressed by estimating the densities from geometric inspection of the unit cells. The use of the total mass as normalizing quantity is a convenient method to compare samples consisting of two or more materials. Both the compressive strength and the compressive modulus were determined by using stress-strain curves of the crushed samples. The average compressive stress was calculated by dividing the reaction force between the rigid wall and the sample by the top surface area of the sample. The ratio of the displacement to the sample height is the strain and the slope of the stress-strain curve in the elastic region has been used for the compressive modulus. On average the elastic strains are varied in the range of 0.02-0.03 strains.

Mechanical performances and energy absorption capabilities of the cellular structures are based on the densification strain at which the plateau regime ends and a sharp increase starts in stress-strain curves. Here, the intersection point of these regions were determined by drawing a straight line for the plateau regime and the slope of densification region. Specific compressive strength, MCF and SEA were determined from the average data points at densification in the range of 0.7, 0.5, 0.5 strains for the hexagonal, re-entrant and AEC re-entrant, respectively.

5.2. Comparison of the specific compressive strength

The regular re-entrant honeycombs possess higher compressive strength than the hexagonal configurations and the introduction of hierarchies in the re-entrant lattice could increase the strength of these structures [1, 30, and 46]. Our hybrid lattice configurations allow the improvement of the compressive strength by modifying the unit cell topologies and adding lightweight materials. Figure 16 shows that hybrid samples provide the highest specific compressive strength compared to the other classes of specimens, no matter which lattice configuration and loading direction are considered. The results also show that the specific compressive strength significantly increases by using very low-density material in hybrid structures. In comparison with the hexagonal samples, the hybrid configurations show a 30% and 34% increase in specific compressive strength over the bulk thickness samples when loading along the *x* and *y*-directions, respectively. Hybrid configurations also provide 12% and

24% more specific compressive strengths than the slotted ones. Hybrid structures with re-entrant and AEC re-entrant shapes display compressive strength efficiencies of 7%, 17% (along the *x*-direction) and 35% and 53% (in the *y*-direction) greater than those shown by the bulk samples. They also display compressive strength efficiencies of 6%, 8% (along the *x*-direction) and 15%, 25% (in the *y*-direction) larger than the slotted samples. The discrepancies of the results related to the compressive strength along the *x* and *y*-directions stem from the different deformation modes [22], which also affect stiffness and the SEA [52].

Multiphase samples show however the worst performance because the hydrogel was squeezed out along the out-of-plane direction during testing. In addition, hybrid structures with re-entrant shape feature an enhanced performance compared to analogous hexagonal configurations; the AEC re-entrant topologies have also the highest specific compressive strengths of 37.2 and 41.5 MPa/kg when loading along the *x* and *y*-directions (Figure 16). These results show that the novel designs with PUR foams inserts are interesting from an engineering perspective when the specific compressive strength needs to be maximized.

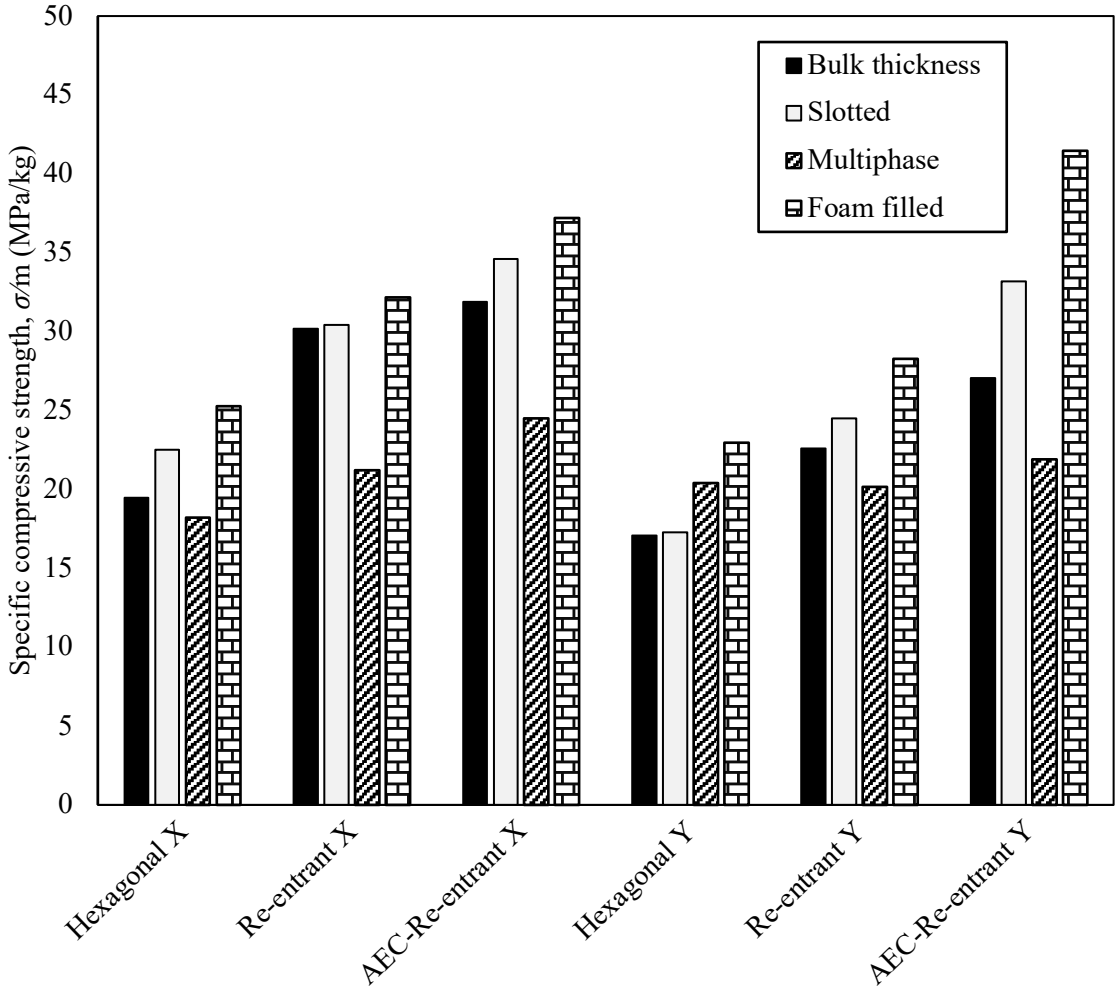

Figure 16: Specific compressive strength.

5.3. MCF comparison

Zhou *et al.* [53] found that re-entrant honeycombs provide higher mean crushing forces than initial peak crushing forces; this allows larger energy absorbing capacities. Tan *et al.* [29] indicated that the MCF of their re-entrant hierarchical honeycombs was improved by up to

298% and 108% compared with conventional re-entrant honeycombs. The MCF performance of the configurations considered here and loaded along the different directions is shown in Figure 17. The re-entrant and AEC re-entrant samples show ~35% increase in MCF performance compared to hexagonal samples along the *x*-direction. There is however no noticeable difference in the MCF performance between the different configurations along the *y*-direction, and this could be explained by the specific deformation modes acting along that direction [22].

The hybrid configurations have larger MCF efficiencies (~5% to 35%) than the slotted and hydrogel-filled samples along the *x* and *y*-directions. The MCFs of hybrid samples with hexagonal, re-entrant and AEC re-entrant shapes are also 13%, 18% and 14% larger than the ones related to the bulk thickness samples along the loading *y*-direction, respectively.

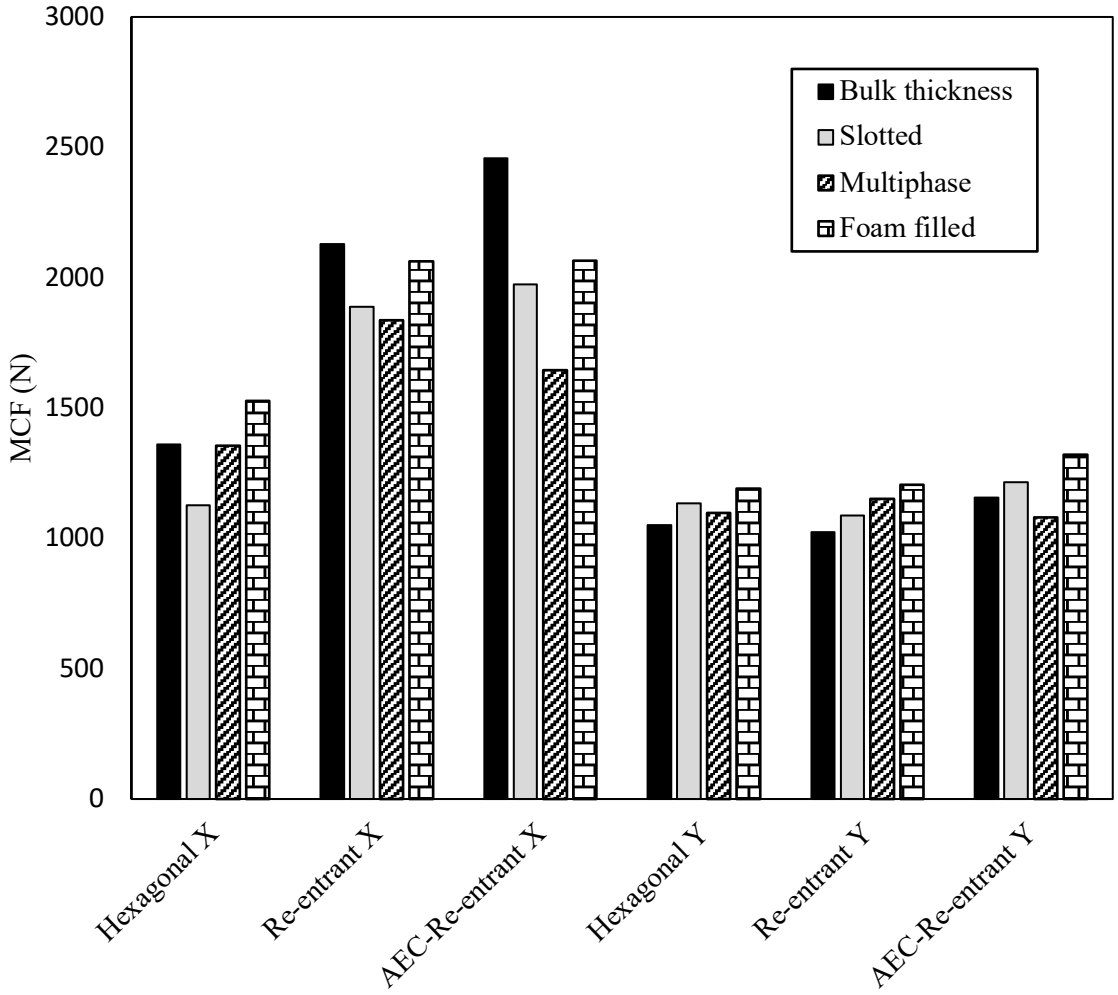

Figure 17: Mean crushing force (MCF)

5.4. SEA comparison

Ingrole *et al.* [1] indicated that re-entrant honeycombs can absorb ~27% more energy than the hexagonal configurations. In addition, the energy absorption capacity could be improved by introducing hierarchies into the re-entrant (e.g., by up to 292% [29]) and hexagonal honeycombs (e.g., by up to 750% [30]). The present study highlights that the proposed hybrid structures can be effective to enhance the energy absorption performance of hierarchical configurations. The SEA performance of the samples with different unit cell configurations loaded along different directions is shown in Figure 18. Bulk thickness samples

with the AEC re-entrant topologies compressed along the *x*-direction had the best energy absorption capacity within the whole family of cellular structures considered here. Multiphase samples had however the lowest specific energy absorption performance due the leaking of hydrogel during quasi-static crushing. Hybrid samples absorb more specific energy than the slotted and hydrogel samples along the *x* and *y*-directions; the SEA of hybrid samples with hexagonal, re-entrant and AEC re-entrant shape features is also 19%, 4% and 6% larger than the one of bulk thickness samples along the loading *y*-direction, respectively. Hybrid configurations also improve the SEA by 6% compared to the bulk thickness samples with hexagonal cellular structures when loaded along the *x*-direction.

Another important result is that the auxeticity causes a reduction of the SEA capacity in hybrid samples compared to the hexagonal ones, and this is due to a ~37% increase of mass. Although re-entrant honeycombs [1] are known to possess more energy dissipation over hexagonal configurations they have larger densities than the regular topologies, and those could dominate the SEA behavior. Asymmetrical configurations appear to be better than conventional re-entrant configuration in terms of the SEA.

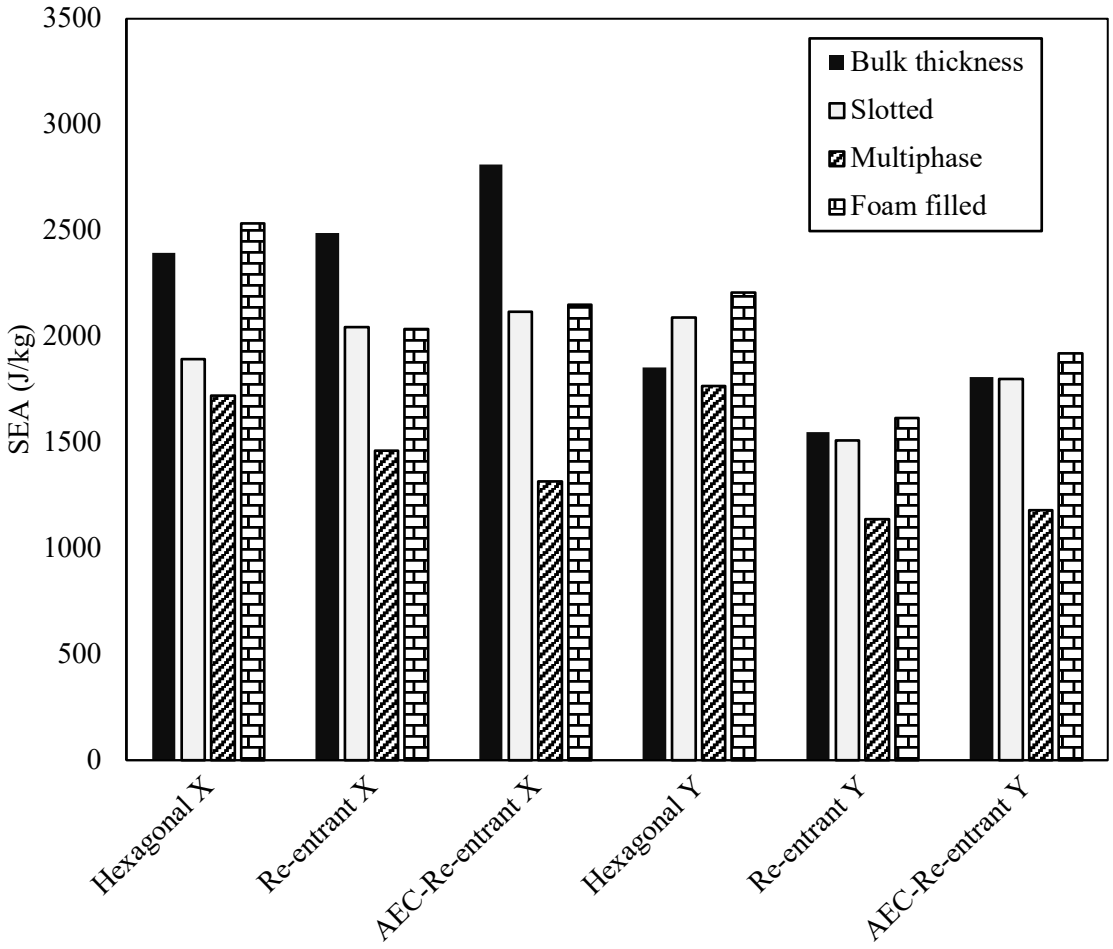

Figure 18: Specific energy absorption (SEA)

5.5. Specific compressive modulus

Figure 19 shows that both slotted and hybrid samples have superior specific modulus compared to the other configurations. This is consistent with similar findings in [29, 30] regarding hierarchical structures. The compressive modulus of hybrid samples along the *x*-direction is increased by 14 % and 11% compared to bulk thickness configurations with hexagonal and re-entrant cellular structures. Out-of-plane leaking of the hydrogel in multiphase samples have

likely caused the decrease of the specific stiffness. The specific modulus of both multiphase and hybrid samples decreases when passing from hexagonal to AEC re-entrant configurations, both for the values associated to the *x* and *y*-directions. The increase of mass is also a likely reason for this reduction. The specific compressive modulus of hybrid samples with re-entrant cellular shapes is ~4% and 2% lower than the one featured by hexagonal cells along the loading *x* and *y*-directions. The samples with AEC re-entrant topologies show ~13% and 59% lower performances. This indicates that the reduction of the cell wall angle θ could be more influential on the stiffness performance of the samples than the resulting increase of mass [52].

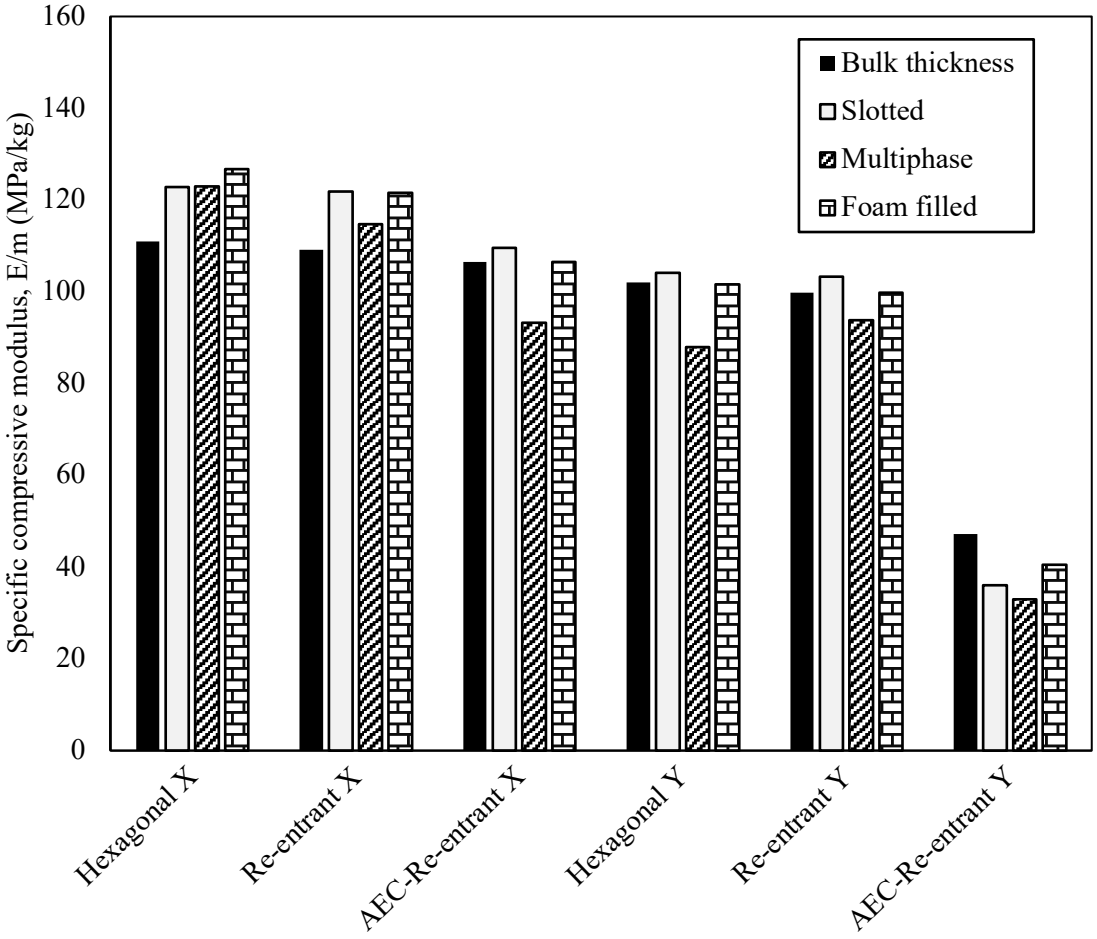

Figure 19: Specific compressive modulus.

6. Parametric studies related to hybrid hierarchical honeycombs

6.1. Finite element simulations

The FE analyses were performed using the LS-DYNA software. Figure 20 shows a 3D view of the FE model of a hybrid sample. A rigid mass crushes the sample at a speed of 3 mm/min. The 'Prescribed motion rigid' tool is used to define the rigid part, the degrees of freedom and the displacement flag. A 'Planar rigid wall' is defined at the bottom of the sample as a boundary.

The PLA-made reinforcement and the PUR foam are modeled by using ELFORM 1 (element formulation option 1) based on constant stress solid elements. The material properties of the PLA-made lattice have been identified by applying the values of the density, Young's modulus, Poisson's ratio, yielding point and stress versus strain data obtained experimentally

into the ‘MAT24 piecewise linear plasticity’ material card. Similarly, the material properties of the PUR foam have been implemented from the experimental material characterization into the ‘MAT63 crushable foam’ material card. Rate sensitivity via damping coefficient has been defined as 0.5. The interaction between the PUR foam and the PLA-made lattice and between the rigid wall and the honeycomb have been defined by using automatic surface-to-surface contact interfaces. Automatic single surface contact algorithms have been also used for each individual foam parts and PLA-made lattice with the coefficient of 0.2.

A mesh convergence study was performed to identify an adequate balance between accuracy and mesh quality. Hybrid samples with foams were modelled using 5 different mesh densities. In these five models the number of elements used were 8853, 10044, 12894, 16305 and 18189. Numerical results have shown that convergence in terms of force versus displacement response was achieved with the finer meshes. The FE modeling of the hybrid sample with a large number of parts (150 foams and a PLA-made lattice) however restricted the minimum element size. A trade-off has been identified with 18189 elements.

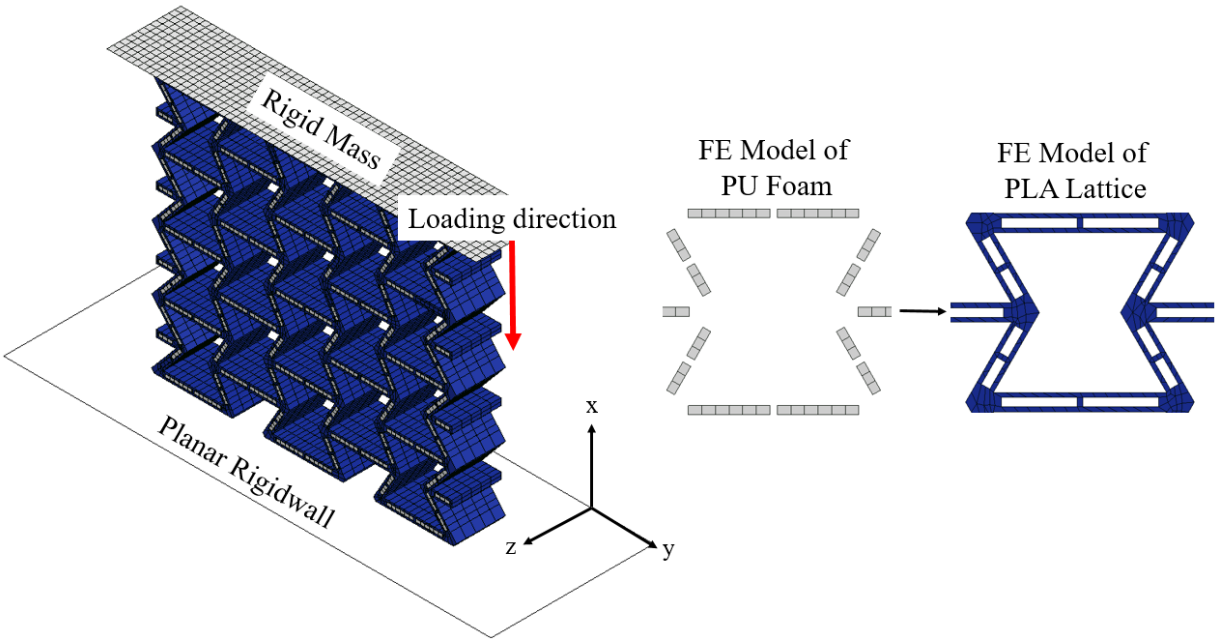

Figure 20: FE modelling of hybrid AEC re-entrant sample.

6.2. Validation of the numerical model

A previous validation of the models used in this work has been performed in [46]. An additional benchmark of the modelling approach has been carried out in this work related to the hybrid structures proposed, and the results are shown in Figure 21. Good agreement can be observed between numerical and experimental results of AEC re-entrant sample having 2 slots (S2-Rectangular) for the three stages of stress-strain curves: linear elastic, plastic collapse plateau and the final densification.

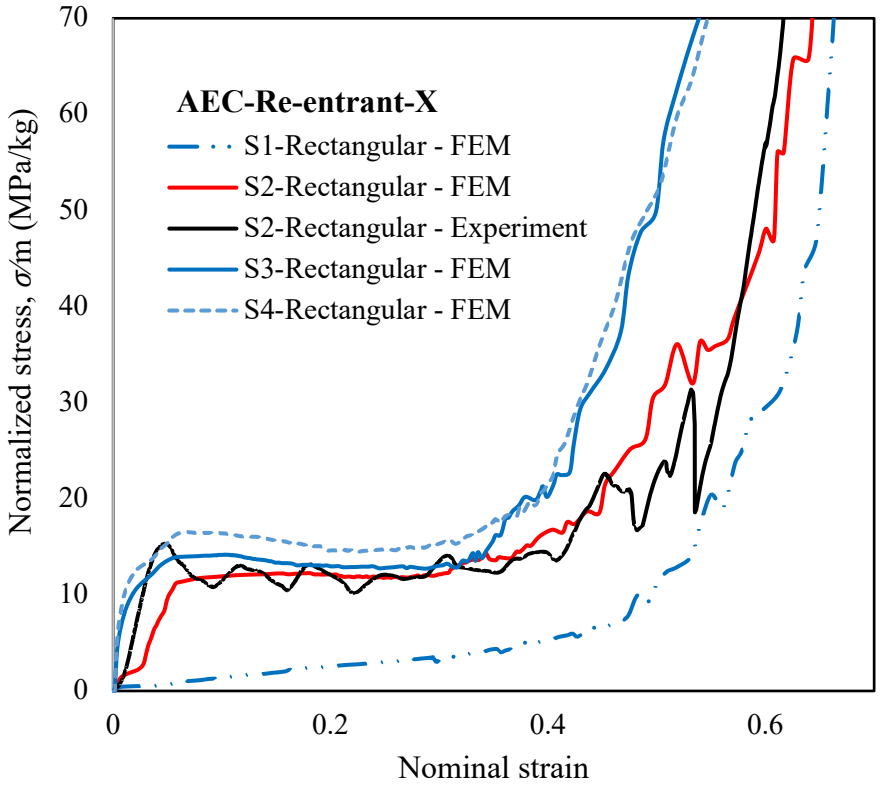

Figure 21: Specific compressive strength vs strain curves of AEC re-entrant sample loading in *x*-direction.

6.3. Parametric analysis

The experimental studies showed that the hybrid samples possess a superior compressive crashworthiness performance compared to the other configurations. The combination of an additive manufactured polymeric structure and the inclusions of a lightweight porous solid provides an increase of mechanical properties of the lattices, especially the ones with auxetic topology. The most common parametric analyses for these cellular structures involve the variation of the internal cell angles [5, 22, 26, 27 and 52] and aspect ratios of the cell ribs [5, 9, 54, 55 and 56]. Apart from those more traditional parameters, we have also previously observed the effects of the hierarchical configurations on the quasi-static crushing performance of the metamaterials presented here. Therefore, the parametric analysis is here focused on the hybrid topologies with varying geometry of the hierarchies in unit cell, but with constant lengths, cell wall angle and thickness of the ribs. The AEC re-entrant topology has been selected as the most mechanically efficient honeycomb configuration; the design parameters consisted in the number of slots present in one rib and the rounding of the corners of both slots in the PLA-made structure and the PUR foam. These modifications were conducted via finite element modeling by taking into consideration the difficulties existing in the manufacturing processes. In the first case, the number of slots on a single rib is varied from 1 to 4 (Figure 22). In the second case, the corners of the slots and foam parts were rounded with a radius of 0.4 mm. The FE simulations indicated that the effect of the radius of rounded corner on the quasi-static crushing performance becomes more visible when the radius is equal or greater than 0.4 mm. Stress concentrations at the sharpened edges of rectangular slots can reduce the strength of the structure under compression loading, and this is the main rationale behind the investigation of the rounding [57]. The reduction in stress concentrations provided by the rounded corners would also help to reduce the onset of failure due to debonding in the weaker parts of the lattice.

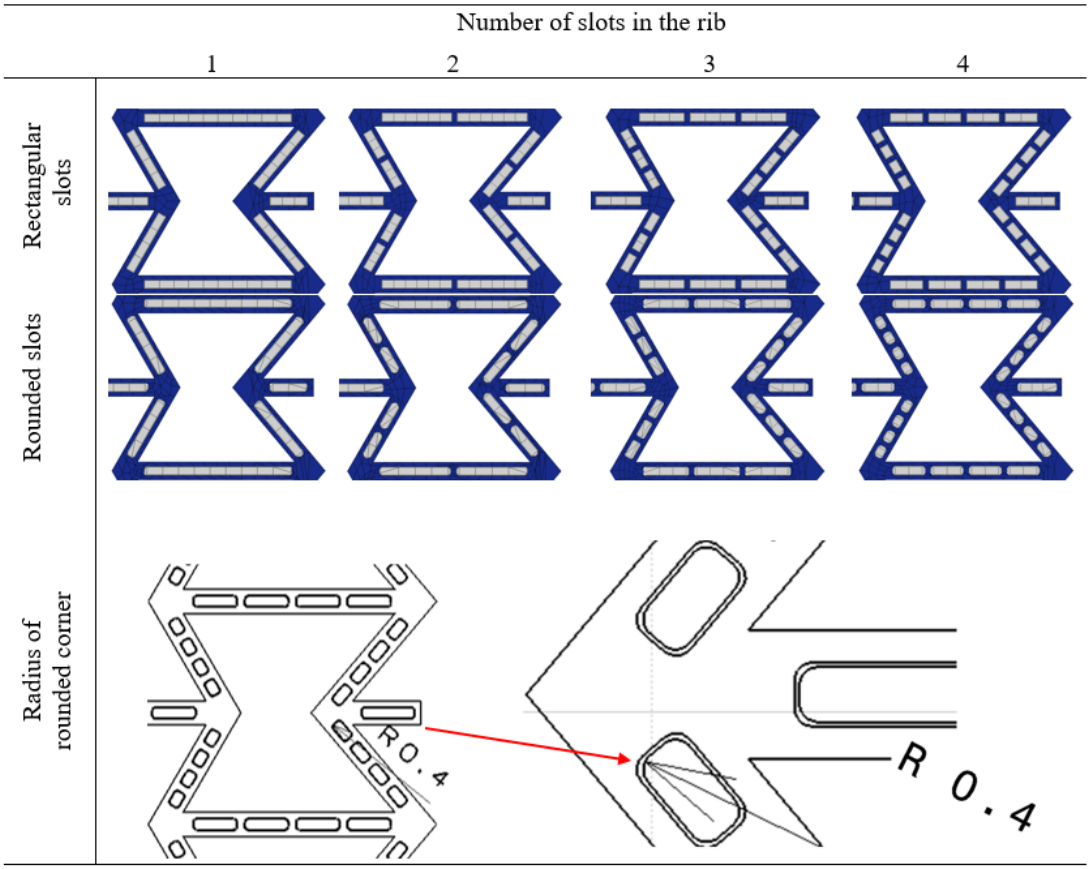

Figure 22: Unit cell configurations of AEC re-entrant samples with and without radius of round by changing number of slots.

Finite element analyses of eight different hybrid samples have been performed and SEA, MCF, specific strength and stiffness calculated. Figure 23 and 24 illustrate the results related to each crashworthiness indicator. The MCF, SEA, Specific compressive modulus and strength values are in the range of 92-2789 N, 61-1650 J/kg and 41-598 MPa/kg and 8-36 MPa/kg, respectively. The results show that the number of slots and the rounded corners of the same slots have remarkable effects. The relative stiffness, SEA and MCF values increase for rising numbers of slots, both in the rectangular and rounded corner cases. Normalized stresses also show an increasing trend when the number of slots is augmented, however the results of samples having 2, 3 and 4 slots are quite close to each other. It is also important to notice that almost all samples with rounded corner have higher specific compressive strength, stiffness, the SEA and the MCF values, except for the case of the S1 samples in terms of specific compressive strength. The deformation mechanism of the rounded S1 sample exhibits a larger global rotation than the rectangular one due to instabilities in the deformation mechanism. The performance of the S1 samples is very reduced compared to those of samples having 2, 3 and 4 slots (more than 300% reduction in any case). The weakness and failure of the ribs of the S1 samples could be the reason of this peculiar behavior in terms of specific compressive strength. Unlike the case of the S1 samples, the adjacent cell walls of the slots and the corner of the unit cells tend to behave as plastic hinges under compression, which reduces the instabilities during the quasi-static crushing. The superiority of the samples with rounded corners over rectangular ones becomes more evident with the increase of the number of slots. The combination of large number of slots per rib, the rounding of their corners and the filling of the slots with foam appears to increase significantly the crashworthiness of the hybrid structures developed in this study. Deformed and non-deformed shapes of the S-4 rounded sample having best performance are indicated in Fig. 25.

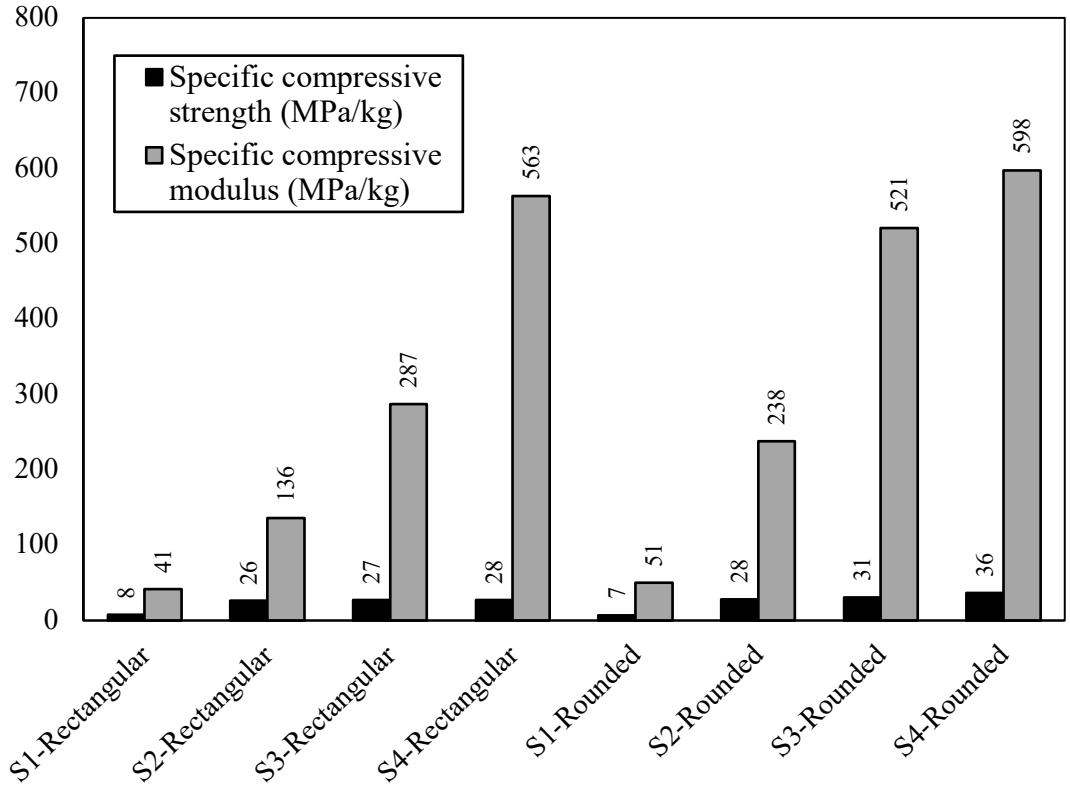

Figure 23: The Specific compressive strength and modulus values of modified hybrid samples.

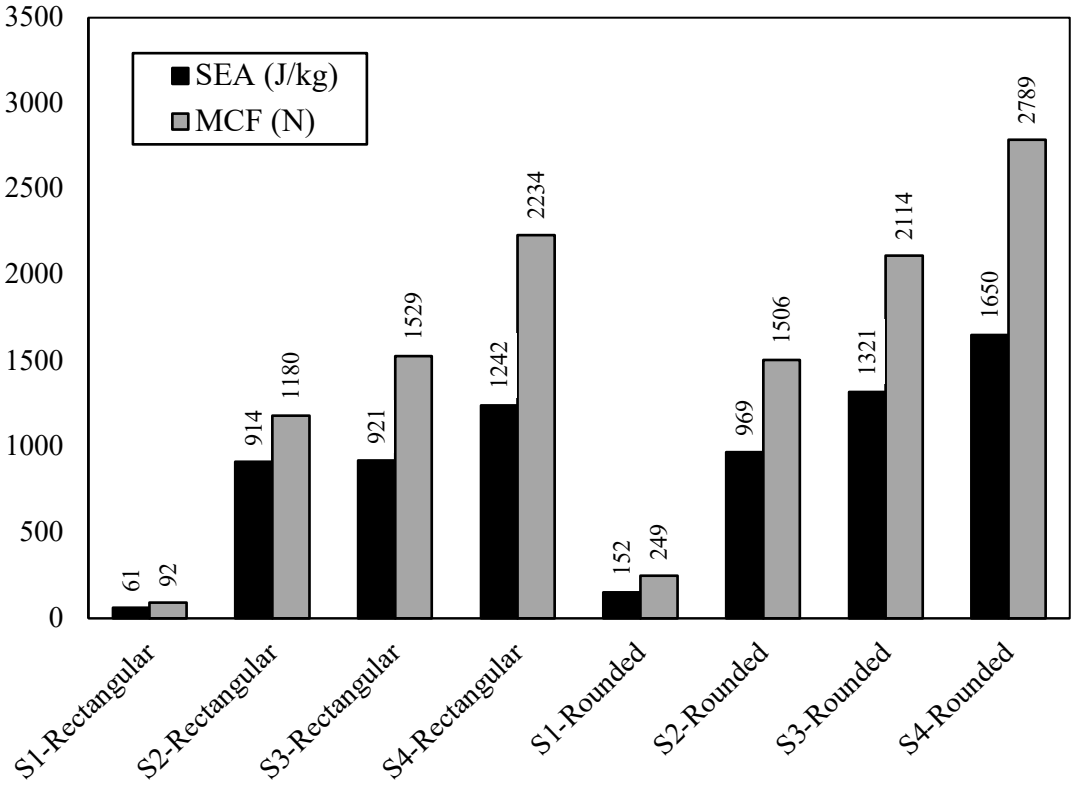

Figure 24: The SEA and MCF values of modified hybrid samples.

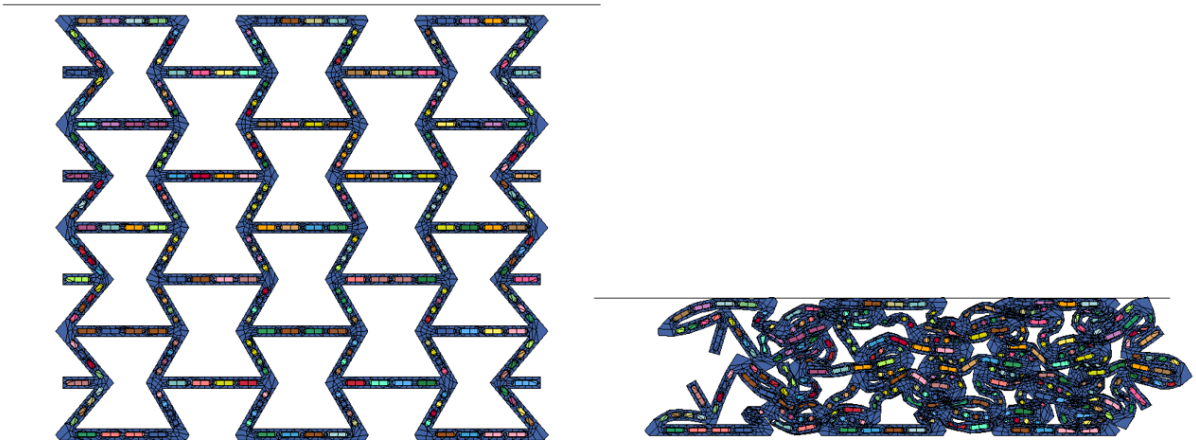

Figure 25: Deformed and non-deformed shapes of the optimum design: S4-rounded sample.

7. Conclusion

This work introduced two novel composite hierarchical cellular shape honeycomb metamaterial designs for crashworthiness applications. The two configurations include the presence of slots in the cell ribs; in one case those slots are filled with PUR foam and in the second case with injected hydrogel. We have looked at the specific compressive strength, stiffness and energy absorption capabilities of these metamaterial configurations made of auxetic and non-auxetic cellular structures (re-entrant, AEC re-entrant and hexagonal).

Experimental tests have been carried out to compare the performance of the novel designs with slots, but also bulk thickness configuration. The multiphase hierarchical samples showed that the non-Newtonian phase filler helps to reduce the instabilities during large deformations of the re-entrant honeycombs under quasi-static crushing. The overall crashworthiness performance of the multiphase samples is worse than the one from the other cases because of the leakage of the hydrogel along the out-of-plane direction. If improvements in the manufacturing process are identified, the stabilization of the deformation mechanism during compressive loading could be however an important aspect for the design of crashworthiness devices.

The results of hybrid samples filled with PUR foam have shown that the specific strength, stiffness and energy absorption of these hybrid structures are higher than those provided by the other configurations (auxetic and non-auxetic). The auxetic configurations (re-entrant and AEC re-entrant) also featured the highest values of specific strength.

The explicit FE parametric analyses performed in this work were made using models related to the hybrid configuration and benchmarked by experimental results. The parameters (number of slots in the ribs and round on the corner of those slots) reflect some aspects of the manufacturing constraints provide by state-of-the-art 3D printing techniques based on FDM. The results showed that those parameters do affect the quasi-static crushing performance, with higher specific stress, stiffness, the SEA and the MCF values increasing in the case of both rectangular and rounded slots. The samples with rounded corner also possess the highest specific stiffness, stress, SEA and MCF values, in particular when auxetic configurations are considered. The crashworthiness of the hybrid metamaterial configurations shown in this work can be improved with the combination of larger number of slots in the ribs and the rounding of their corners.

Acknowledgment

Support for this work has been provided by the Scientific and Technological Research Council of Turkey (TUBITAK) under Fellowship Number 2214-A with application number 1059B141800436. The work has been also supported by the University of Bristol and the Bristol Composites Institute (ACCIS).

References

[1] Ingrole A, Hao A, and Liang R 2017 Design and modeling of auxetic and hybrid honeycomb structures for in-plane property enhancement *Materials & Design* **117** 72-83.

[2] Simpson J and Kazancı Z 2020 Crushing investigation of crash boxes filled with honeycomb and re-entrant (auxetic) lattices *Thin-Walled Structures* **150** 106676.

[3] Usta F, Ertaş OF, Ataalp A, Türkmen HS, Kazancı Z and Scarpa F 2019 Impact behavior of triggered and non-triggered crash tubes with auxetic lattices *Multiscale and Multidisciplinary Modeling, Experiments and Design* **2** 119-127.

[4] Hu LL and Deng H 2015 Indentation resistance of the re-entrant hexagonal honeycombs with negative Poisson's ratio, *Materials Research Innovations* **19** 442-445.

[5] Lira C and Scarpa F 2010 Transverse shear stiffness of thickness gradient honeycombs *Composites Science and Technology* **70** 930-936.

[6] Easey N, Chuprynyuk D, Musa WM, Bangs A, Dobah Y, Shterenlikht A and Scarpa F 2019 Dome-shape auxetic cellular metamaterials: manufacturing, modeling, and testing *Frontiers in Materials* **6** 86

[7] Alderson K, Alderson A, Anand S, Simkins V, Nazare S, Ravirala N 2012 Auxetic warp knit textile structures *Physica status solidi (b)* **249** 1322-1329.

[8] Mohsenizadeh M, Gasbarri F, Munther M, Beheshti A, Davami K 2018 Additively-manufactured lightweight Metamaterials for energy absorption *Materials & Design* **139** 521-530.

[9] Rayneau-Kirkhope D 2018 Stiff auxetics: Hierarchy as a route to stiff, strong lattice based auxetic meta-materials *Scientific reports* **8** 1-10.

[10] Grima JN and Evans KE 2006 Auxetic behavior from rotating triangles. Journal of materials science **41** 3193-3196.

[11] Grima JN, Farrugia PS, Gatt R and Attard D 2008 On the auxetic properties of rotating rhombi and parallelograms: A preliminary investigation *Physica status solidi (b*) **245** 521-529.

[12] Attard D, and Grima JN 2008 Auxetic behaviour from rotating rhombi. physica status solidi (b) **245** 2395-2404/

[13] Grima JN, Gatt R, Ellul B, and Chetcuti E 2010 Auxetic behaviour in non-crystalline materials having star or triangular shaped perforations *Journal of Non-Crystalline Solids* **356** 1980-1987.

[14] Wang ZP, Poh LH, Zhu Y, Dirrenberger J and Forest S 2019 Systematic design of tetra-petals auxetic structures with stiffness constraint *Materials & Design* **170** 107669.

[15] Gibson LJ, Ashby MF, Schajer GS and Robertson CI 1982 The mechanics of two-dimensional cellular materials *Proceedings of the Royal Society of London. A. Mathematical and Physical Sciences* **382** 25-42.

[16] Lakes R 1987 Foam structures with a negative Poisson's ratio *Science* **235** 1038-1041.

[17] Choi JB and Lakes RS 1992 Non-linear properties of polymer cellular materials with a negative Poisson's ratio *Journal of Materials Science* **27** 4678-4684.

[18] Masters IG and Evans KE 1996 Models for the elastic deformation of honeycombs *Composite structures* **35** 403-422.

[19] Gibson LJ and Ashby MF 1999 Cellular solids: structure and properties. *Cambridge university press*.

[20] Evans KE and Alderson A 2000 Auxetic materials: functional materials and structures from lateral thinking! *Advanced materials* **12** 617-628.

[21] Scarpa F, Panayiotou P and Tomlinson G 2000 Numerical and experimental uniaxial loading on in-plane auxetic honeycombs *The Journal of Strain Analysis for Engineering Design* **35** 383-388.

[22] Scarpa F and Tomlinson G 2000 Theoretical characteristics of the vibration of sandwich plates with in-plane negative Poisson's ratio values *Journal of Sound and Vibration* **230** 45-67.

[23] Grima JN, Alderson A and Evans KE 2005 Auxetic behaviour from rotating rigid units *Physica status solidi (b)* **242** 561-575.

[24] Bezazi A, Scarpa F and Remillat C 2005 A novel centresymmetric honeycomb composite structure *Composite Structures* **71** 356-364.

[25] Dong Z, Li Y, Zhao T, Wu W, Xiao D and Liang J 2019 Experimental and numerical studies on the compressive mechanical properties of the metallic auxetic reentrant honeycomb *Materials & Design* **182** 108036.

[26] Xiao D, Kang X, Li Y, Wu W, Lu J, Zhao G and Fang D 2019 Insight into the negative Poisson's ratio effect of metallic auxetic reentrant honeycomb under dynamic compression *Materials Science and Engineering*: *A* **763** 138151.

[27] Tatlier MS 2019 A numerical study on energy absorption of re-entrant honeycomb structures with variable alignment *International Journal of Crashworthiness* 1-9.

[28] Liu W, Wang N, Luo T and Lin Z 2016 In-plane dynamic crushing of re-entrant auxetic cellular structure *Materials & Design* **100** 84-91.

[29] Tan HL, He ZC, Li KX, Li E, Cheng AG and Xu B 2019 In-plane crashworthiness of re-entrant hierarchical honeycombs with negative Poisson’s ratio *Composite Structures* **229** 111415.

[30] Chen Y, Li T, Jia Z, Scarpa F, Yao CW and Wang L 2018 3D printed hierarchical honeycombs with shape integrity under large compressive deformations *Materials & Design* **137** 226-234.

[31] Alomarah A, Masood SH, Sbarski I, Faisal B, Gao Z and Ruan D 2020 Compressive properties of 3D printed auxetic structures: experimental and numerical studies *Virtual and Physical Prototyping* **15** 1-21.

[32] Hou Y, Neville R, Scarpa F, Remillat C, Gu B and Ruzzene M 2014 Graded conventional-auxetic Kirigami sandwich structures: Flatwise compression and edgewise loading *Composites Part B: Engineering* **59** 33-42.

[33] Ge Z, Hu H and Liu Y 2013 A finite element analysis of a 3D auxetic textile structure for composite reinforcement *Smart materials and structures* **22** 084005.

[34] Jayanty S, Crowe J and Berhan L 2011 Auxetic fibre networks and their composites *Physica status solidi (b)* **248** 73-81.

[35] Jopek H and Strek T 2015 Thermal and structural dependence of auxetic properties of composite materials *Physica status solidi (b)* **252** 1551-1558.

[36] Scarpa FL, Remillat C and Landi FP and Tomlinson GR 2000 Damping modelization of auxetic foams *In Smart Structures and Materials 2000: Damping and Isolation International Society for Optics and Photonics* **3989** 336-343.

[37] Murray GJ and Gandhi F 2013 Auxetic honeycombs with lossy polymeric infills for high damping structural materials *Journal of intelligent material systems and structures* **24** 1090-1104.

[38] Barbarino S, Pontecorvo ME and Gandhi FS 2012 Cellular honeycomb-like structures with internal buckling and viscous elements for simultaneous load-bearing and dissipative capability *In Smart Materials, Adaptive Structures and Intelligent Systems American Society of Mechanical Engineer*s **45103** 395-405.

[39] Aumjaud P, Smith C and Evans KE 2015 A novel viscoelastic damping treatment for honeycomb sandwich structures *Composite Structures* **119** 322-332.

[40] Boucher MA, Smith CW, Scarpa F, Rajasekaran R and Evans KE 2013 Effective topologies for vibration damping inserts in honeycomb structures *Composite Structures* **106** 1-14.

[41] Sloan MR, Wright JR and Evans KE 2011 The helical auxetic yarn–a novel structure for composites and textiles; geometry, manufacture and mechanical properties *Mechanics of Materials* **43** 476-486.

[42] Quan C, Han B, Hou Z, Zhang Q, Tian X and Lu TJ 2020 3D printed continuous fiber reinforced composite auxetic honeycomb structures *Composites Part B: Engineering* **187** 107858.

[43] Subramani P, Rana S, Oliveira DV, Fangueiro R and Xavier J 2014 Development of novel auxetic structures based on braided composites *Materials & Design* **61** 286-295.

[44] Xu W, Yan B, Hu D and Ma P 2020 Preparation of auxetic warp-knitted spacer fabric impregnated with shear thickening fluid for low-velocity impact resistance *Journal of Industrial Textiles* 1528083720927013.

[45] Fu K, Wang H, Chang L, Foley M, Friedrich K and Ye L 2018 Low-velocity impact behaviour of a shear thickening fluid (STF) and STF-filled sandwich composite panels *Composites Science and Technology* **165** 74-83.

[46] Usta F, Scarpa F and Türkmen HS 2020 Edgewise compression of novel hexagonal hierarchical and asymmetric unit cells honeycomb metamaterials *Materials Today Communications* 101102.

[47] Armstrong JP, Burke M, Carter BM, Davis SA and Perriman AW 2016 3D bioprinting using a templated porous bioink *Advanced healthcare materials* **5** 1724-1730.

[48] ASTM International, ASTM D638-14, *Standard Test Method for Tensile Properties of Plastics*.

[49] ASTM D1621-00 *Standard test method for compressive properties of rigid cellular plastics*.

[50] Toksoy AK 2003 Quasi-static axial compression behavior of empty and polystyrene foam filled aluminum tubes Master's thesis, Izmir Institute of Technology.

[51] Yin H, Huang X, Scarpa F, Wen G, Chen Y and Zhang C 2018 In-plane crashworthiness of bio-inspired hierarchical honeycombs *Composite Structures* **192** 516-527.

[52] Chen J, Chen W, Hao H, Huan S and Tao W 2020 Mechanical behaviors of 3D re-entrant honeycomb polyamide structure under compression *Materials Today Communications* 101062.

[53] Zhou Z, Zhou J and Fan H 2017 Plastic analyses of thin-walled steel honeycombs with re-entrant deformation style *Materials Science and Engineering: A* **688** 123-133.

[54] Hou X, Deng Z and Zhang K 2016 Dynamic crushing strength analysis of auxetic honeycombs *Acta Mechanica Solida Sinica* **29** 490-501.

[55] Hou J, Li D and Dong L 2018 Mechanical behaviors of hierarchical cellular structures with negative Poisson's ratio *Journal of Materials Science* **53** 10209-10216.

[56] Li D, Yin J, Dong L and Lakes RS 2016 Numerical analysis on mechanical behaviors of hierarchical cellular structures with negative Poisson's ratio *Smart Materials and Structures* **26** 025014.

[57] Sharma DS 2012 Stress distribution around polygonal holes *International Journal of Mechanical Sciences* **65** 115-124.